*36th EPS Conference on Plasma Phys. Sofia, June 29 - July 3, 2009 ECA Vol.**33E**, P-2.195 (2009)*

Collective behaviors of fast ions accelerated by Ion Cyclotron Resonance Heating

C. Di Troia, S. Briguglio, A. Cardinali, G. Fogaccia, M. Marinucci, G. Vlad, F. Zonca

Associazione Euratom-ENEA sulla Fusione, C.R. Frascati,

C.P. 65 - I-00044 - Frascati, Rome, Italy

Introduction

This work focuses on fast ion transport caused by collective modes and the corresponding evolution of meso-scale fluctuations in burning plasma. More specifically, we analyze these problems in the FAST (Fusion Advanced Studies Torus) [1] H-mode reference scenario, a conceptual design proposal for a EU ITER Satellite tokamak. As explained in [2], FAST approaches dimensionless parameters $\rho_H^* = \rho_{H,L}/a$ ($\rho_{H,L}$ is the fast ions Larmor radius and a the minor radius of the torus), $\beta_H = 8\pi P_H/B^2$ (P_H is the fast ion scalar pressure and B the intensity of the magnetic field) and geometry of ITER in a smaller device. In this way it can investigate some of the relevant α particle physics of ITER, using a D plasma with a ^3He minority heated by Ion Cyclotron Resonance Heating (ICRH). Here and in the following the subscript H stands for suprathermal minority (Hot) particles. In this work, we briefly discuss perpendicular and parallel temperatures radial profiles, charactreristic of the FAST H-mode reference scenario, and the spatial density radial distributions of the energetic ion minority tail fraction, respectively denoted by $T_{H,\perp}(r), T_{H,\parallel}(r)$ and $n_H(r)$, with r being the minor radius coordinate. We then simulate the fast ion behavior using HMGC [3], a 3-D hybrid MHD-Gyrokinetic simulation code. Linear and saturated spectra are presented together with numerical simulation results on fast particle transport due to Alfvén mode excitation for moderate toroidal mode numbers, $n = 4$ and 8.

The FAST H-mode reference scenario

The FAST H-mode reference scenario is achieved by dominant ICRH. To simulate L-H mode transition we used the 1D-transport code JETTO [4], the full wave EM code TORIC [5], that can investigate the ICRH injected power redistribution , and SSQLFP [6], a Fokker-Planck solver, used to follow the evolution of the density n_H and the pressures $P_{H,\parallel} = n_H T_{H,\parallel}$ and $P_{H,\perp} = n_H T_{H,\perp}$. The L-H transition was modeled by three iterations of JETTO and TORIC/SSQLFP. In the first iteration, TORIC used temperature profiles, density distribution and safety factor $q(r)$ obtained by JETTO for the ohmic phase. The power density deposition profiles (PDDPs), hence obtained by TORIC, are used as input for the 2^{nd} iteration, where JETTO simulates the heating phase after ICRH onset, eventually yielding the L-H transition. At the 3^{rd} and final iteration, the

Bohm-gyroBohm shear independent transport model [7], more appropriate for the H-mode, is used in the further JETTO simulation. TORIC computes PDDPs for the last time (because the steady state is reached) from the JETTO density and temperature profiles. Simulation results of

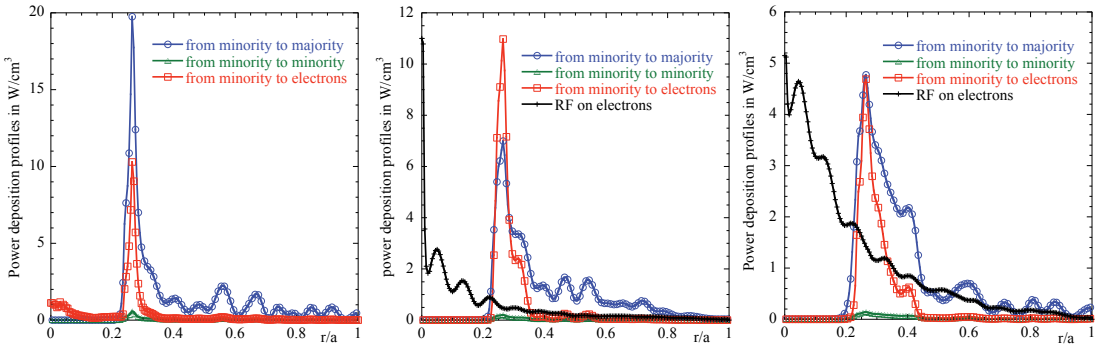

Fig. 1: PDDPs obtained with TORIC, for the three iterations described in the text, for D ions, electrons (collisional plus direct RF heating) and minority ions accounting for collisional power redistribution among species.

H-mode scenario formation are reported in Fig. 1.

Fast particle results

The interaction between energetic ions and Alfvén modes is simulated using HMGC that properly takes into account kinetic excitations and nonlinear dynamics with a Particle In Cell approach. This code can handle the case of an anisotropic Maxwellian as an initial fast ion velocity space distribution function, such as that expected for ICRH. We choose

$$F_H \propto n_H(r) \exp\left[-\frac{E-\mu B_{min}(r)}{T_{H,*}(r)} - \frac{E}{T_{H,\perp}(r)}\right], \tag{1}$$

as the initial phase space distribution, with the radius $r(\psi)$ given in terms of the poloidal flux variable ψ and $B_{min}(r) = \min_\theta B(r,\theta)$ with θ the poloidal angle. E is the kinetic energy and μ the magnetic moment. $T_{H,*}$ measures the temperature anisotropy: $1/T_{H,*} = 1/T_{H,\|} - 1/T_{H,\perp}$. The function in eq. (1) is normalized such as to obtain the correct profiles: $n_H(r) = \int \langle F_H \rangle d\theta/(2\pi)$, $P_{H,\perp}(r) = m_H \int \langle \mathbf{v}_\perp^2 F_H \rangle d\theta/(4\pi)$ and $P_{H,\|}(r) = m_H \int \langle v_\|^2 F_H \rangle d\theta/(2\pi)$ with angular brackets indicating velocity space integration. $F_H = F_H(r,E,\mu)$ is function of constants of motion E and μ except for r dependences. Thus F_H is not an exact equilibrium distribution function because it is built from TORIC output, which neglects finite orbit width effects. This intrinsic limitation is expected to be less severe at long wavelengths (compared with the finite orbit width) and/or strong drive, for which it is essentially the local mode growth that dictates the dynamic evolution [8]. According to our simulations, this condition appears to be fulfilled

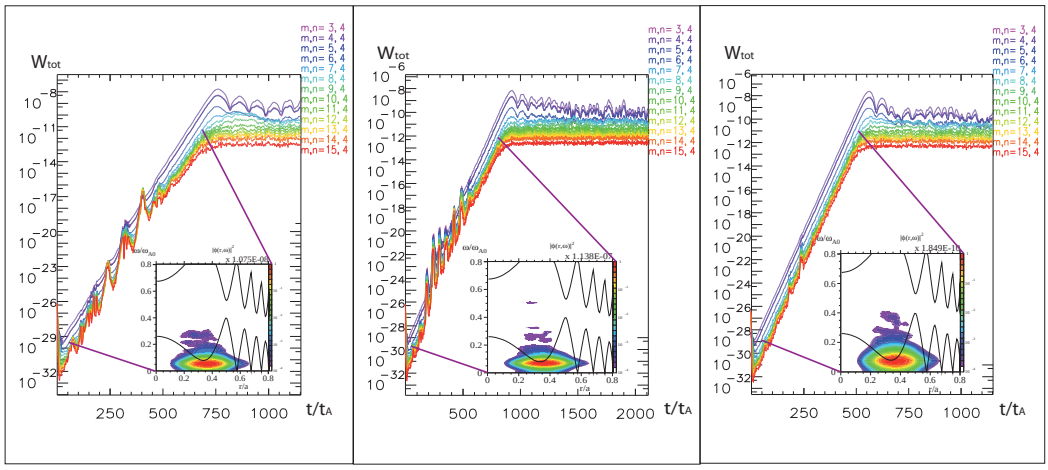

Fig. 2: Radially integrated magnetic energy of the perturbed toroidal $n = 4$ and poloidal m components vs time in Alfvén units (the corresponding mode intensity logarithmic (ω, r)-contour plot during the linear phase is also shown) for an ICRH power of 18 MW, 30 MW (nominal) and 43 MW, respectively from left to right.

when considering moderate n ($n \lesssim 8$) and sufficiently high ICRH injected power. As depicted in the right plot in Fig. 2. The figure shows a set of simulations with constant temperature and density profiles that has been done by changing $\beta_{H,\perp} = 8\pi P_{H,\perp}/B^2$ in order to simulate the effect of different ICRH injected power. For $n = 4$, we show the radially integrated magnetic energy of the perturbed poloidal m components vs time given in units of the Alfvén time (the corresponding mode intensity logarithmic (ω, r)-contour plot during the linear phase is also shown) for an ICRH power of 18 MW, 30 MW (nominal) and 43 MW, moving from left to right of Fig. 2.

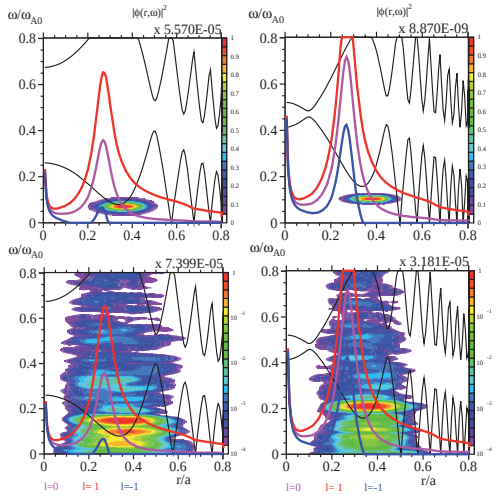

Fig. 3: Alfvén mode intensity (ω, r)-contour plots for $n = 4$ (left) and $n = 8$ (right) during the linear (top) and non-linear (bottom) instability growth phase. The toroidal continuous spectrum and the frequencies of the precession, $\bar{\omega}_{dH}$, and precession-bounce, $\bar{\omega}_{dH} \pm l\omega_{BH}$, resonance are also shown.

For the nominal case, the Alfvén mode intensity (ω, r)-contour plots for $n = 4$ (top-left) and $n = 8$ (top-right) during the linear instability growth phase are presented in Fig. 3. The shear Alfvén continuous spectrum and the frequencies of the precession, $\bar{\omega}_{dH}$, and precession-bounce, $\bar{\omega}_{dH} \pm \omega_{BH}$, resonance are also shown. The corresponding nonlinear saturation phases are given at the bottom of the same figure, where the appearance of a richer spectrum of modes can be seen. The left part of Fig. 4 shows the radial

mode structure for the $n = 8$ mode in the poloidal cross section for both linear (top) and non-linear saturation (bottom) phases, plotted as contours of the scalar potential fluctuation (note that the circular plasma cross section is imposed by HMGC model equilibrium geometry).

On the right side of Fig. 4 we show the effect of $n = 8$ Alfvénic modes on supra-thermal tail ion transport. Radial β_H distributions are initially lowered by $\sim 44\%$ and broadened, indicating a "prompt relaxation" of F_H due to finite magnetic drift orbit width. β_H values during the subsequent linear phase (top-right in Fig. 4) are compared with the final nonlinear saturated phase (bottom-right in Fig. 4): a macroscopic reduction of energetic ions is observed.

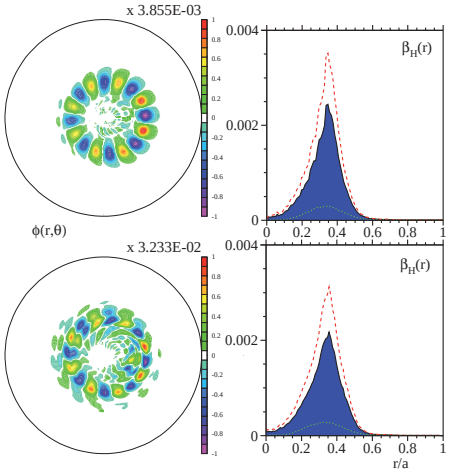

Fig. 4: Radial mode structure for the $n = 8$ mode in the poloidal cross section for both linear (top-left) and nonli- near saturation (bottom-left) phases. Radial β_H, $\beta_{H,\perp}$ (red dashed line) and $\beta_{H,\parallel}$ (green dotted line) distributions during the linear phase (top-right) and the nonlinear saturated phase (bottom-right).

In conclusion, numerical simulation results confirm the theoretical prediction [8] that the Alfvén fluctuation spectrum in FAST will be dominated by a dense spectrum of modes with characteristic frequencies and radial locations leading to fast particle transport and suggesting that radial n_H profiles will play a crucial role. FAST and ITER are expected to behave similarly for higher n. These high-n cases will be reported in a separate work.

References

[1] A. Pizzuto et al. “The Fusion Advanced Studies Torus (FAST): a proposal for an ITER satellite facility in support of the development of fusion energy” submitted to Nucl. Fusion 2009.

[2] G. Calabrò et al., Nucl Fusion **49** 055002 (2009)

[3] S. Briguglio et al., Phys. Plasmas **2** 3711 (1995); S. Briguglio et al., Phys. Plasmas **5** 3287 (1998)

[4] G. Cenacchi and A.Taroni, ENEA Report RT/TIB/88/5 (1988)

[5] M. Brambilla, Plasma Phys. Control. Fusion **41** 1 (1999)

[6] M. Brambilla, Nucl. Fusion **34** 1121 (1994)

[7] G. Vlad et al., Nucl. Fusion **38** 557 (1998)

[8] F. Zonca et al., Plasma Phys. Control. Fusion **48** B15 (2006); L. Chen and F. Zonca, Nucl. Fusion **47** S727 (2007); L. Chen, Plasma Phys. Control. Fusion **50** 124001(2008)